Degradation of periodic multilayers as seen by small-angle x-ray scattering and x-ray diffraction

2002 J. Phys.: Condens. Matter 14 10021

(http://iopscience.iop.org/0953-8984/14/43/301)

INSTITUTE OF PHYSICS PUBLISHING JOURNAL OF PHYSICS: CONDENSED MATTER

J. Phys.: Condens. Matter **14** (2002) 10021–10032 PII: S0953-8984(02)38469-8

Degradation of periodic multilayers as seen by small-angle x-ray scattering and x-ray diffraction

David Rafaja,[1,3,4], Hartmut Fuess[1], Daniel Šimek[2], Lenka Zdeborová[2] and Václav Valvoda[2]

[1] Institute for Materials Science, Darmstadt University of Technology, Petersenstr. 23, D-64287 Darmstadt, Germany
[2] Department of Electronic Structures, Charles University, Ke Karlovu 5, CZ-121 16 Prague, Czech Republic

E-mail: rafaja@karlov.mff.cuni.cz

Received 21 June 2002, in final form 25 September 2002
Published 18 October 2002
Online at stacks.iop.org/JPhysCM/14/10021

Abstract

The capabilities of small-angle x-ray scattering (SAXS) and wide-angle x-ray diffraction (XRD) to recognize structural changes in periodic multilayers were compared on Fe/Au multilayers with different degrees of structural degradation. Experimental results have shown that both methods are equally sensitive to the multilayer degradation, i.e., to the occurrence of non-continuous interfaces, to short-circuits in the multilayer structure and to the multilayer precipitation. XRD yielded additional information on the multilayer crystallinity, whilst SAXS could better recognize fragments of a long-range periodicity (remnants of the original multilayer structure). Changes in the multilayer structure were initiated by successive annealing at 200 and 300 °C. Experimental data were complemented by numerical simulations performed using a combination of optical theory and the distorted wave Born approximation for SAXS or the kinematical Born approximation for XRD.

1. Introduction

The combination of small-angle x-ray scattering (SAXS) with wide-angle x-ray diffraction (XRD) is employed as an efficient tool for investigation of the real structure in periodic multilayers [1]. The complementarity of these two techniques is evident especially if crystalline multilayers are the subject of the study. SAXS yields information on electron density and thickness of individual layers, as well as on roughness and morphology of interfaces [2, 3]. XRD better recognizes short-range periodicity, such as inter-atomic distances. Thus, XRD

[3] On leave from: The Department of Electronic Structures, Charles University, Ke Karlovu 5, CZ-121 16 Prague, Czech Republic.
[4] Author to whom any correspondence should be addressed.

primarily yields information on interplanar spacing and its fluctuations, which are related to the degree of the multilayer crystallinity. For a medium bi-layer thickness ($\Lambda < 100$ Å), the XRD patterns taken near the first Bragg diffraction maximum also contain information on the mean bi-layer thickness and on the average number of atomic planes within the respective layer. The mean thickness of the respective layer, which results from the above parameters, can be directly compared with the thickness obtained from SAXS. Thus, the combination of SAXS and XRD improves substantially the reliability of the structural model that is especially useful for highly disturbed metallic multilayers [4, 5].

Since the giant magnetoresistance effect was observed in granular alloys [6, 7], not only well developed multilayers but also multilayers with a high degree of structure degradation became interesting for magnetic applications. The granular structure develops either during the deposition process [8] or afterwards by supplying an external energy to the multilayer system. For the latter, laser irradiation [9] or soft annealing [10, 11] were used alternatively. Moreover, successive annealing was applied to modify the size of granules [12–14], as the size distribution of magnetic granules is believed to play a crucial role for the magnetic properties of such materials [15].

In a recent paper [16], we showed the effect of interface discontinuity on SAXS. The interface discontinuity can be regarded as a first step in the multilayer degradation, which possibly results in precipitation of discontinuous layers after a further temperature treatment. This work shows evolution of the small-angle and wide-angle diffraction patterns during multilayer degradation, and compares the sensitivities of SAXS and XRD to the structural changes in individual stages of the multilayer degradation. As a model system, Fe/Au multilayers were selected due to a low mutual miscibility of iron and gold at 400 °C [17] and due to a high diffraction contrast of both species.

2. X-ray scattering on highly disturbed multilayers

Symmetrical SAXS (x-ray reflectivity, XRR) is described by optical theory [18], which was proved to be equivalent to the dynamical diffraction theory [19]. For calculation of reflectivity curves, the recursive numerical approach [2] is typically employed, that is based on the Parratt optical formalism [20] taking into account a decrease of the interface reflectivity due to interface roughness [21]. The multilayer discontinuity decreases the Fresnel reflection coefficients of individual interfaces and modifies the optical path of x-rays within the multilayer [16]. The related decrease of XRR at individual interfaces attenuates primarily the Bragg-like maxima observed in the reflectivity curve. Therefore, the discontinuous interfaces have a similar effect on the reflectivity curve like changes in the electron density of individual layers if they are combined with an increase of the interface roughness.

In order to explain phenomena that are observed in the non-specular (diffuse) scattering on multilayers, the semi-kinematical distorted wave Born approximation (DWBA) must be employed [22, 23]. The differential cross section of the diffuse scattering, which is proportional to the scattered intensity, is a product of the intensity of the incoming and outgoing waves and of a two-dimensional Fourier transform of a correlation function $C_j(x, y)$. The index j denotes individual interfaces. The intensity of radiation at the respective interface is determined by the Fresnel transmission and reflection coefficients of the successive interfaces in the multilayer stack. The two-dimensional Fourier transform of the correlation function [23]

$$\tilde{F}_j(q_x, q_y) = \int_S \mathrm{d}x\, \mathrm{d}y\, C_j(x, y) \mathrm{e}^{-\mathrm{i}(xq_x + yq_y)} \tag{1}$$

is calculated over the irradiated area S. $C_j(x, y)$ describes correlation of interface corrugations.

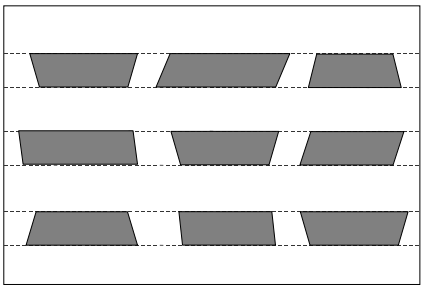

Figure 1. Model of a multilayer with non-continuous interfaces. Dashed lines show original positions of interfaces in a continuous multilayer.

For non-continuous interfaces, the integration in (1) is to be performed over the continuous parts of the interfaces [16]

$$\tilde{F}_j(q_x, q_y) = \sum_k \int_S \mathrm{d}x\,\mathrm{d}y\, C_j(x, y)\mathrm{e}^{-\mathrm{i}(xq_x+yq_y)}\Omega_{k,j}(x, y), \tag{2}$$

for which $\Omega_{k,j}(x, y)$ is equal to unity (otherwise $\Omega_{k,j}(x, y) = 0$). The index k labels the continuous regions of the interface j.

Wide-angle XRD on periodic multilayers with continuous interfaces is described within the kinematical diffraction theory [1]. Periodic multilayers with non-continuous interfaces can be regarded as consisting of precipitates of one atomic species, embedded in a matrix of the other atomic species (figure 1). Thus, the total scattered amplitude can be divided into two parts, the first one being attributed to the matrix (M), the second one to the precipitates (P).

$$E = \int_V \rho E_0(\vec{r})\mathrm{e}^{\mathrm{i}\vec{q}\cdot\vec{r}}\,\mathrm{d}\vec{r} = \int_M \rho_M E_0(\vec{r})\mathrm{e}^{\mathrm{i}\vec{q}\cdot\vec{r}}\,\mathrm{d}\vec{r} + \int_P \rho_P E_0(\vec{r})\mathrm{e}^{\mathrm{i}\vec{q}\cdot\vec{r}}\,\mathrm{d}\vec{r}. \tag{3}$$

In (3), ρ_M and ρ_P are the electron density of the matrix and the electron density of the precipitates, respectively. E_0 is the respective amplitude of the incoming wave; $\vec{r}$ is the position vector, $\vec{q}$ the diffraction vector. Assuming constant amplitude within each precipitate, the last scattering term can be simplified.

$$\int_P \rho_P E_0(\vec{r})\mathrm{e}^{\mathrm{i}\vec{q}\cdot\vec{r}}\,\mathrm{d}\vec{r} = \sum_j \int_P \rho_P E_0(\vec{R}_j + \vec{r}')\mathrm{e}^{\mathrm{i}\vec{q}\cdot(\vec{R}_j+\vec{r}')}\,\mathrm{d}\vec{r}' = \sum_j E_0(\vec{R}_j)\mathrm{e}^{\mathrm{i}\vec{q}\cdot\vec{R}_j}\int_P \rho_P \mathrm{e}^{\mathrm{i}\vec{q}\cdot\vec{r}'}\,\mathrm{d}\vec{r}'. \tag{4}$$

$\vec{R}_j$ is the position of the jth precipitate; $\vec{r}'$ denotes the position vector inside the precipitate. Indeed, the same approach can be applied to the matrix, as the matrix can be understood as a continuous layer with the precipitates excluded.

$$\int_M \rho_M E_0(\vec{r})\mathrm{e}^{\mathrm{i}\vec{q}\cdot\vec{r}}\,\mathrm{d}\vec{r} = \int_V \rho_M E_0(\vec{r})\mathrm{e}^{\mathrm{i}\vec{q}\cdot\vec{r}}\,\mathrm{d}\vec{r} - \sum_j E_0(\vec{R}_j)\mathrm{e}^{\mathrm{i}\vec{q}\cdot\vec{R}_j}\int_P \rho_M \mathrm{e}^{\mathrm{i}\vec{q}\cdot\vec{r}'}\,\mathrm{d}\vec{r}'. \tag{5}$$

Consequently, the total amplitude (3) is given by the following scattering terms.

$$E = \int_V E_0(\vec{r})\rho_M \mathrm{e}^{\mathrm{i}\vec{q}\cdot\vec{r}}\,\mathrm{d}\vec{r} + \sum_j E_0(\vec{R}_j)\mathrm{e}^{\mathrm{i}\vec{q}\cdot\vec{R}_j}\int_P (\rho_P - \rho_M)\mathrm{e}^{\mathrm{i}\vec{q}\cdot\vec{r}'}\,\mathrm{d}\vec{r}'. \tag{6}$$

As usual in the kinematical Born approximation, the integral $\int \rho \mathrm{e}^{\mathrm{i}\vec{q}\cdot\vec{r}'}\,\mathrm{d}\vec{r}'$ can be calculated for isolated atoms and added up over all atomic positions $\vec{P}_k$.

$$\int \rho \mathrm{e}^{\mathrm{i}\vec{q}\cdot\vec{r}'}\,\mathrm{d}\vec{r}' = \sum_k \int \rho \mathrm{e}^{\mathrm{i}\vec{q}\cdot(\vec{P}_k+\vec{r}'')}\,\mathrm{d}\vec{r}'' = \sum_k \mathrm{e}^{\mathrm{i}\vec{q}\cdot\vec{P}_k}\int \rho \mathrm{e}^{\mathrm{i}\vec{q}\cdot\vec{r}''}\,\mathrm{d}\vec{r}'' = \sum_k f_k \mathrm{e}^{\mathrm{i}\vec{q}\cdot\vec{P}_k}. \tag{7}$$

This corresponds to the well known kinematical representation of a structure factor in terms of the atomic scattering factors f_k. If the amplitude of the incoming wave, E_0, is constant through the whole multilayer (which is safely fulfilled for wide-angle XRD because of negligible absorption of x-rays in thin samples), the total scattered amplitude can be expressed in terms of structure factors corresponding to the matrix, which is extended over the whole sample, and to precipitates having the differential scattering factor $(f_P - f_M)$.

$$E = E_0\left\{\sum_{\text{Sample}} f_M \mathrm{e}^{\mathrm{i}\vec{q}\cdot\vec{P}_M} + \sum_j \left[\mathrm{e}^{\mathrm{i}\vec{q}\cdot\vec{R}_j}\sum_k (f_P - f_M)\mathrm{e}^{\mathrm{i}\vec{q}\cdot\vec{P}_{j,k}}\right]\right\}. \tag{8}$$

Structure factors in (8) grow linearly with the volume of the respective part of the multilayer. Assuming constant thickness of a flat sample, the structure factors are linearly proportional to area and, consequently, to the continuity c of interfaces.

$$E = E_0\left[(1-c)F_{M(S)} + c\sum_j F_{P-M}\mathrm{e}^{\mathrm{i}\vec{q}\cdot\vec{R}_j}\right]. \tag{9}$$

In (9), $F_{M(S)}$ is the structure factor of the matrix and F_{P-M} the structure factor of the precipitates. Both are calculated for the same area of the sample. In binary multilayers with non-continuous interfaces studied in symmetrical geometry, the scattering amplitude can easily be calculated using the formula

$$E = E_0\left[(1-c)F_M + c\sum_j \mathrm{e}^{\mathrm{i}qz_j}(F_{Aj} + F_{Bj}\mathrm{e}^{\mathrm{i}qt_{Aj}})\right], \tag{10}$$

where F_M is the structure factor of the matrix-like (discontinuous) parts of the sample and the sum expresses the structure factor of the remaining multilayer. Obviously, for a multilayer with continuous interfaces ($c = 1$), equation (10) yields the same structure factor as derived in [1]

$$F_{\text{ML}} = \sum_j \mathrm{e}^{\mathrm{i}qz_j}(F_{Aj} + F_{Bj}\mathrm{e}^{\mathrm{i}qt_{Aj}}). \tag{11}$$

z_j are positions of the B/A interfaces and t_{Aj} the thickness of layer A_j. Consequently, multilayers with non-continuous interfaces can be considered as a specific case of multilayers with continuous interfaces, in which regions with a well developed multilayer structure contribute to the total diffracted intensity together with the matrix-like regions.

$$I = |E_0|^2\{(1-c)^2|\langle F_M\rangle|^2 + c^2|\langle F_{\text{ML}}\rangle|^2 + 2c(1-c)\,\mathrm{Re}(\langle F_M F^*_{\text{ML}}\rangle)\}. \tag{12}$$

The symbol $\langle\cdots\rangle$ means the mean value, the asterisk the complex conjugate and Re the real part of a complex number. The first and the second term in (12) describes the scattering by matrix and by precipitates, respectively. The last term in (12) results from mutual coherence of waves scattered on continuous layers or matrix and on precipitates. A numerical example (figure 2) illustrates the evolution of diffraction pattern at increasing discontinuity of interfaces. Already at 20% interface discontinuity, the contribution of the 'mixed' term $2c(1-c)\,\mathrm{Re}(\langle F_M F^*_{\text{ML}}\rangle)$ enhances considerably the reflection from the matrix. At 40% interface discontinuity, the reflection from the matrix dominates in the diffraction pattern. The simulations were done for an Fe/Au (26 Å/25 Å) × 10 multilayer deposited on a 60 Å gold buffer. The size of the coherent domains (crystallites) in the gold matrix was assumed to be 200 Å. The crystallite size modifies primarily the shape of the peaks corresponding to the matrix.

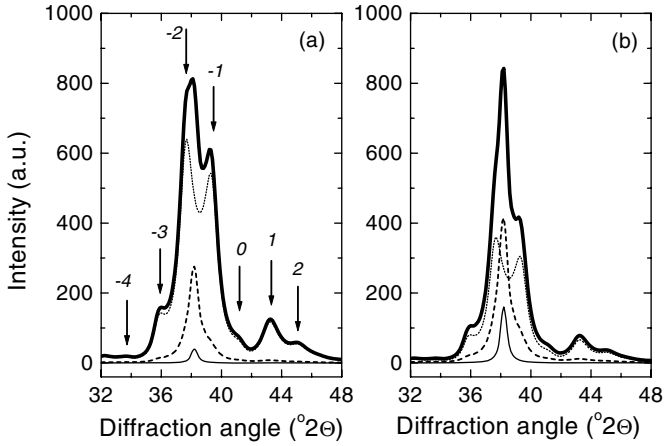

Figure 2. XRD patterns simulated for 20% (a) and 40% (b) interface discontinuity. Total diffracted intensity (broad solid curve) is composed of intensity diffracted by the matrix (——) and precipitates (· · · · · ·) and of the cross term $2\mathrm{Re}(F_M F^*_{P-M})$ (- - - -). The satellites from precipitates are labelled by their order.

3. Experimental details

Fe/Au multilayers with the basic parameters (26 Å Fe/24 Å Au) × 10 and (70 Å Fe/21 Å Au) × 13 were deposited by RF diode sputtering onto quartz glass substrates [25]. Prior to the multilayer deposition, the substrates were covered with a gold buffer having the thickness of 100 Å. To destroy the original multilayer structure, samples were annealed for 2 h at 200 °C in inert atmosphere, which was argon of 5 N purity. As no substantial changes were observed after the initial annealing, additional annealing was performed at 300 °C (in the same atmosphere). The successive annealing time was 2 h for the sample with thin iron layers, or 2 and 4 h for the sample with thick iron layers.

SAXS and XRD experiments were performed on a two-circle diffractometer (Seifert XRD 3003 PTS). Radiation of a 1.6 kW tube with Cu anode was reflected by Goebel mirror to achieve a high intensity of the primary beam at a sufficient planarity of the incoming wave (needed for SAXS). A slit located behind the Goebel mirror reduced the width of the primary beam and decreased slightly its angular divergence. After scattering on the sample, the radiation was transmitted to a secondary graphite monochromator and diffracted into the detector. To improve the resolution of the diffractometer, another slit was inserted between the sample and the graphite monochromator. For SAXS, the first slit had the width of 0.1 mm, the second slit 0.05 mm. For the wide-angle XRD experiments, the slits were wider open (0.3 and 0.5 mm) to achieve a higher intensity of the scattered radiation, because in polycrystalline multilayers a low diffracted intensity is always a more critical issue than the angular resolution.

4. Experimental results

4.1. Sample Fe/Au (26 Å/24 Å) × 10

The complementariness of SAXS and XRD is illustrated on parameters of the structure model obtained using either technique (table 1). For the reflectivity curve fitting, the model of multilayers with non-continuous interfaces [16] was applied. Each layer was characterized by

Table 1. Structure parameters of the multilayer Fe/Au (26 Å/24 Å) × 10 before and after annealing as obtained using a combination of XRR and XRD.

	As deposited		2 h/200 °C	
	XRR	XRD	XRR	XRD
t (Fe) (Å)	26.5	25.6	26.5	27.0
t (Au) (Å)	24.0	24.6	22.0	27.8
Λ (Å)	50.5	50.2	48.5	54.8
d (Fe) (Å)		2.031		2.027
d (Au) (Å)		2.359		2.353
δ (Å)		0.09		0.13
σ (Fe) (Å)	6.5	1.0	7.0	2.0
σ (Au) (Å)	6.5	1.2	8.0	2.4
σ_{surf} (Å)	6.5		9.0	
Continuity (%)	90	100	85	80

a continuity, thickness and interface roughness. Electron densities of individual layers were not refined, as no interdiffusion was anticipated in the Fe/Au system with the very limited mutual miscibility of species. Symmetrical XRD patterns were fitted by using equation (12). The 'Thomson-like' intensity E_0 was refined within the scale factor. Individual structure factors for the residual multilayer F_{ML} and for the matrix F_M were calculated using the theoretical approach given in [1]. The parameters, which are typically obtained from the structure model, are the mean layer thickness t, interlayer distance t(interlayer), fluctuation in the number of atomic layers within individual layers (discrete roughness) σ, interplanar spacing d and its fluctuation δ, which is reciprocally proportional to the degree of crystallinity. As the phase of both structure factors in (12) is related to the substrate, there is no phase shift between waves scattered on matrix and precipitates. Thus, the last term in (12) does not introduce new interference effects into the diffraction pattern.

The virgin multilayer Fe/Au (26 Å/24 Å) × 10 had a well developed superstructure with a regular layer thickness. This particular result was obtained from the reflectivity curve fitting (figure 3, on the left) and confirmed both by existence of pronounced dynamical Bragg-like resonant lines [26], observed in the reciprocal space map, and by a small discrete roughness calculated from the XRD pattern. Another feature, which was observed in the small-angle reciprocal space map taken on this multilayer, was a high amount of resonant diffuse scattering (RDS). Strong RDS indicates a high correlation of interface corrugations [3]. The fitting of the longitudinal scans (Ω-scans) yielded a lateral correlation length of 210 Å; the corrugations were vertically correlated through the whole multilayer. The high correlation of the interface corrugations allows the discrete roughness (i.e., the variation in the number of atomic planes within individual layers) to be small, although the interface roughness calculated from XRR (i.e., the variation in the positions of individual interfaces) is high. This phenomenon is documented in table 1, as the interface roughness σ is much higher from SAXS than from XRD. The reflectivity curve fitting yielded 10% multilayer discontinuity. No interface discontinuity was detected by XRD. The XRD pattern could successfully be fitted using a standard multilayer model assuming continuous interfaces. Individual layers were crystalline having only small fluctuations δ in the interplanar spacing d (figure 3, on the right).

Annealing for 2 h at 200 °C caused extinction of the Kiessig oscillations and broadening of the Bragg-like maxima in the reflectivity curve (figure 3, on the left) that was interpreted as a larger fluctuation of the layer thickness. Correspondingly, the Bragg-like resonant lines

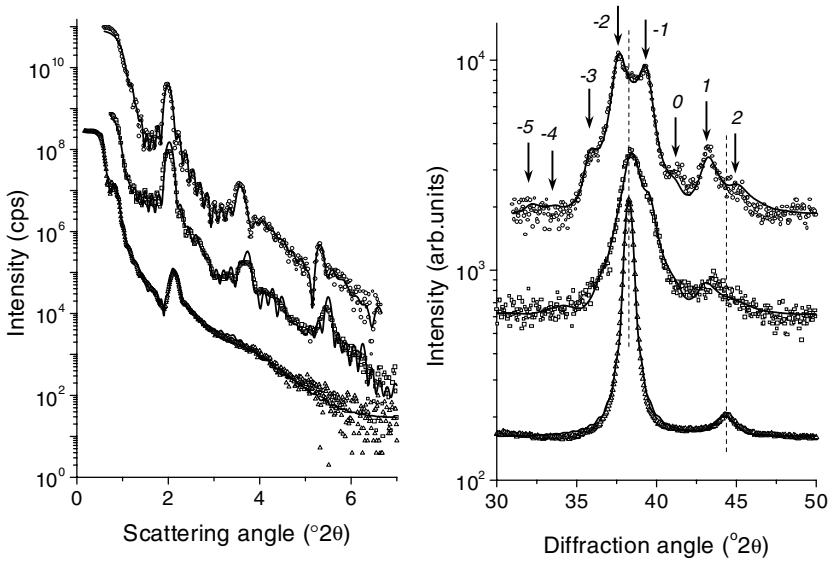

Figure 3. Left: reflectivity curves (○) measured on sample Fe/Au (26 Å/24 Å) × 10 and the respective fit (——). Right: symmetrical XRD patterns taken with the same sample (the diffracted intensities are normalized). Dashed lines show positions of the diffraction lines 111 (Au) and 110 (Fe). From top to bottom: the as-deposited multilayer, the multilayer annealed for 2 h at 200 °C and the multilayer annealed additionally for 2 h at 300 °C.

disappeared from the reciprocal space map. The interface discontinuity calculated from the reflectivity curve increased slightly to approximately 15%. In the XRD pattern, a rapid decay of multilayer satellites was observed after the annealing (figure 3, on the right). This effect could clearly be attributed to the interface discontinuity, because the calculated vertical size of coherent domains in the matrix-like regions was 200 Å, which exceeded the buffer thickness (100 Å) safely.

Annealing for another 2 h at 300 °C almost destroyed the multilayer structure. Only the 111 reflection from gold and the 110 reflection from iron were observed in the XRD pattern. On the other hand, XRR could still recognize the basic periodicity of the original multilayer, which was 49 Å as estimated from the position of the first Bragg maximum in the lowermost reflectivity curve (figure 3). However, the reflectivity curve fitting did not yield any other reasonable parameter, which would characterize the real structure of the multilayer.

4.2. Sample Fe/Au (70 Å/21 Å) × 13

Refinement of the reflectivity curves and the symmetrical XRD pattern (figure 4) yielded parameters that are summarized in table 2. The differences in the individual layer thickness, obtained from SAXS and XRD, are within experimental accuracy. A larger difference was only noted for interface roughness. Nevertheless, the difference in the interface roughness, calculated from the XRR curve and from the XRD pattern, is smaller than in the previous sample. This is due to much lower vertical correlation of corrugations in the Fe/Au (70 Å/21 Å) × 13 multilayer, which was proved by a lower intensity of RDS observed in asymmetrical SAXS. Fitting of the diffuse scattering (figure 5) yielded the vertical correlation length of 800 Å, assuming exponential decay of the vertical correlation [3]. The calculated lateral correlation length was 180 Å for the Au/Fe and 380 Å for the Fe/Au interface. A low

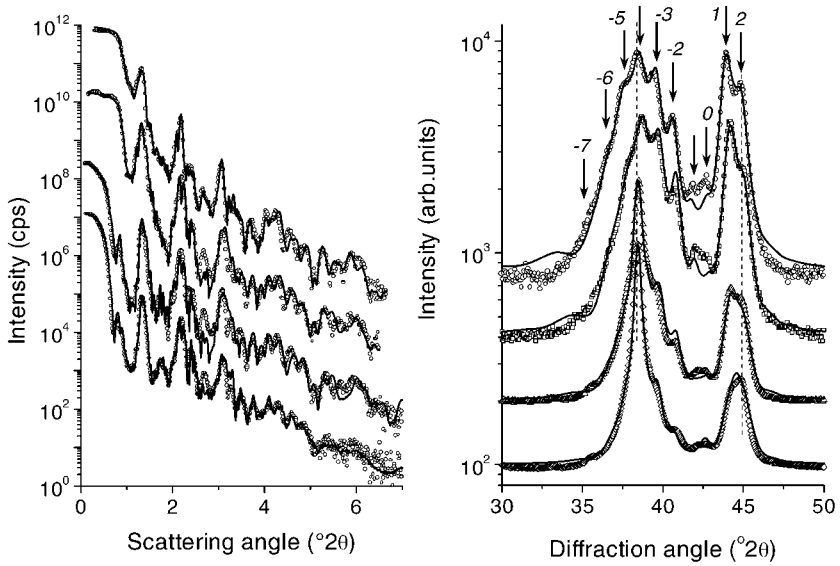

Figure 4. Left: reflectivity curves (O) measured on sample Fe/Au (70 Å/21 Å) × 13 and the respective fit (——). Right: symmetrical XRD patterns measured on the same sample (the diffracted intensities are normalized as in the previous figure). Dashed lines show positions of the diffraction lines 111 (Au) and 110 (Fe). The satellites are marked by arrows. From top to bottom: the as-deposited multilayer, the multilayer annealed for 2 h at 200 °C and the multilayer annealed additionally for 2 and 4 h at 300 °C.

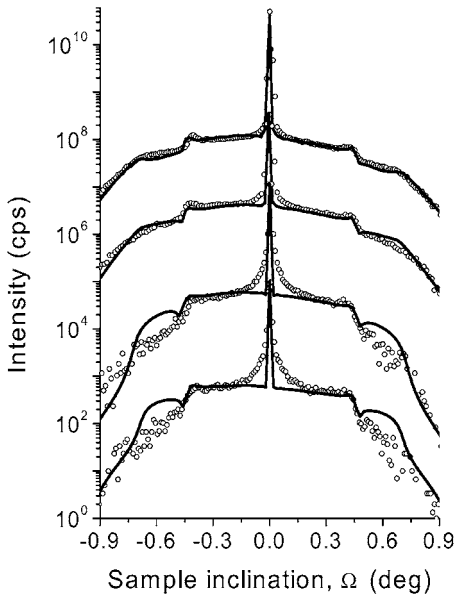

Figure 5. Longitudinal (Ω) scans taken at $2\theta = 2.17°$ (the second Bragg maximum in the reflectivity curve) on the sample Fe/Au (70 Å/21 Å) × 13. From top to bottom: the as-deposited multilayer, the multilayer annealed for 2 h at 200 °C and the multilayer annealed additionally for 2 and 4 h at 300 °C.

Table 2. Structure parameters of a successively annealed multilayer with the original composition Fe/Au (70 Å/21 Å) × 13 as obtained using the combination of XRR and XRD. The annealing time and temperature noted in the heading are valid for the respective annealing phase. $\rho(\mathrm{Fe}_1)$ is the relative electron density of the uppermost Fe layer, which was affected by oxidation during the annealing.

	As deposited		2 h/200 °C		2 h/300 °C		4 h/300 °C	
	XRR	XRD	XRR	XRD	XRR	XRD	XRR	XRD
t (Fe) (Å)	69.7	63.5	68.1	63.0	69.6	62.9	69.9	61.8
t (Au) (Å)	20.4	24.3	21.6	24.8	20.8	25.9	19.4	25.8
t (interlayer) (Å)		2.2		2.1		2.1		2.1
Λ (Å)	90.1	90.0	89.7	89.9	90.4	90.9	89.3	89.7
d (Fe, 110) (Å)		2.036		2.031		2.028		2.027
d (Au, 111) (Å)		2.339		2.318		2.319		2.327
δ (Å)		0.076		0.070		0.067		0.040
σ (Fe) (Å)	8.0	4.5	12.0	5.0	11.5	6.5	12.0	6.5
σ (Au) (Å)	9.5	5.0	11.5	5.5	11.0	6.0	13.0	7.5
σ_{surf} (Å)	12.0		16.0		16.0		20.0	
$\rho(\mathrm{Fe}_1)$	1.0		1.0		0.7		0.6	
Continuity (%)	100	100	100	100	100	100	90	90

vertical correlation in thick layers is anticipated because the interface roughness is controlled rather by crystallization or re-crystallization of individual layers than by transmitting the roughness from substrate or buffer to the surface.

Successive annealing (2 h/200 °C, 2 h/300 °C and 4 h/300 °C) caused a relaxation of the lattice deformation in iron, improved crystallinity of all individual layers and increased the interface and surface roughness. Large d-spacing of iron observed in the virgin sample indicated a lattice deformation of 4.4×10^{-3} caused by a compressive residual stress. After annealing the sample for 6 h at 300 °C (preceded by 2 h at 200 °C), the interplanar spacing of iron (d_{110}) matched well with the intrinsic value of 2.0268 Å [27]. Thus, the residual stress in iron relaxed. In our multilayer model, the degree of crystallinity is reciprocally proportional to the parameter δ, which expresses the width of the Gaussian distribution of the interplanar spacing. In the course of annealing, the parameter δ decreased to approximately one-half of its original value, which indicates an improvement of crystallinity. However, the most rapid crystallization was connected with a steep increase of the interface and surface roughness and with onset of the interface discontinuity.

Onset of the interface discontinuity was recognized by SAXS and XRD after the same annealing (6 h/300 °C), although the XRD patterns showed much larger changes than the reflectivity curves (figure 4). The temperature-induced changes in the reflectivity curves were rather subtle, as they correspond to small changes in the interface roughness and discontinuity. However, the largest changes in the XRD patterns are related to re-crystallization of the buffer layer. Consequently, a significant effect in the XRD patterns is an increase of intensity of the Au 111 reflection. In later stages of the annealing process, intensity and broadening of this diffraction line corresponded to a vertical size of coherent domains, which is equal to the buffer thickness. Only the successive annealing for 6 h at 300 °C preceded by 2 h at 200 °C caused changes in the XRR curve as well as in the XRD pattern, which could be perceived as indicators of the multilayer discontinuity. For the XRD pattern, the apparent effect, related to the increasing multilayer discontinuity, was an increase of the intensity of the Fe 110 reflection. The final size of the coherent Fe domains was 300 Å. Increasing intensity of Bragg maxima,

which arise on large coherent crystallites of either multilayer component, implied a decrease of intensity of superstructure satellites. Thus, the accuracy of structure parameters obtained from the XRD patterns declined rapidly.

In the reflectivity curves measured on annealed samples, a shift of the edge of the total external reflection (TER) to lower angles was observed, which was accompanied by occurrence of a peak immediately behind the edge of TER. This effect was described by Parratt [20] as the 'reflection trap' and explained theoretically by the presence of spongy aggregates of crystallites (or oxidized crystallites) at the sample surface. Accordingly, the reflectivity curves taken after annealing up to 2 h at 300 °C were fitted using the structure model assuming an oxidized near-surface iron layer (the relative electron density of the first iron layer was refined together with other free parameters of the model). After the final annealing, a large decrease of the Bragg-like maxima was observed that could not be described simply by a decrease of the electron density (oxidation) of the surface and by an increase of the interface roughness, but the structure model must have involved a discontinuity of internal interfaces. As the electron density correlates strongly with the interface discontinuity in the refinement [16], it is not reasonable to refine these parameters simultaneously, but an appropriate structure model involving only a few free parameters must be considered prior to fitting. Other indicators of the interface discontinuity are the increase of the diffuse scattering and the broadening of the specular peak. Both effects are illustrated on the longitudinal scans shown in figure 5. The dominant effect is the broadening of the specular peak. This can theoretically be explained by the decreasing size of the continuous regions ($\Omega_{k,j}(x, y)$ in (2)), which causes concentration of the diffuse scattering at the Bragg maxima, see [16] for more details.

5. Discussion

Differences in the SAXS and XRD patterns taken on the annealed multilayers can be explained with the following consideration. At the beginning of the multilayer precipitation, the interfaces are locally interrupted, but still reflecting. For the small-angle scattering this means that the dynamical scattering dominates over the kinematical one (scattering on individual precipitates). Thus, the changes in the reflectivity curve are subtle and can sufficiently be described using modified Fresnel reflection coefficients [16]. The effect of the non-continuous reflecting interfaces on XRR is comparable with changes caused by a slightly different electron density in all layers combined with a higher interface roughness. Fundamental changes in the reflectivity curve are anticipated when the discontinuous layers turn to precipitates with non-reflecting horizontal boundaries. XRD recognizes first the changes in the layer crystallinity. Intensity diffracted by the matrix is particularly enhanced if the matrix becomes coherent through the whole sample.

Still, SAXS and XRD recognized the interface discontinuity at nearly the same level of the temperature-induced structural changes, although the XRD patterns change apparently much more than the reflectivity curves. However, the dominant changes in the XRD patterns are related to the growth of crystallites and to the relaxation of structure faults in individual layers. Particularly for multilayers deposited on buffer, for which the composition is identical with the composition of either layer, the increase of the crystallite size in the buffer has a similar effect on the diffraction pattern like interface discontinuity. Therefore, the interface discontinuity can safely be distinguished from re-crystallization of the buffer only if the calculated crystallite size evidently exceeds the thickness of the buffer layer. The buffer thickness is reliably determined from the reflectivity curve, as SAXS is not sensitive to the local atomic ordering.

The thicknesses of individual layers and the periodicity of the basic motif were obtained from XRR and XRD with a similar reliability. As the wide-angle XRD is sensitive to the

atomic ordering, the XRD pattern contains additional information on the interplanar spacing and its fluctuation, which cannot be obtained from the reflectivity curves. Thus, XRD can recognize residual stresses in the multilayer, which are not accessible by SAXS. On the other hand, roughness of individual interfaces and the interface continuity are better determined from SAXS, because of its non-sensitivity to the local atomic ordering (to the degree of crystallinity).

The differences between the interface roughness obtained from SAXS (from the reflectivity curve measurement) and from XRD have already been mentioned in section 4.1. As a possible reason for these differences, the unlikeness of the respective definition of the interface roughness was considered. Another reason could be the much smaller lateral coherence length for XRR than for XRD, which means that XRD probes the interface quality locally. As all the multilayers were investigated using the same experimental setup (using SAXS and XRD, respectively), we can expect a constant difference between the interface roughness obtained from SAXS and XRD, which is in disagreement with our observations. Thus, SAXS yields a more reasonable information on the interface roughness, because the interface roughness obtained from SAXS is related to the absolute position of the respective interface, which is not true for XRD. Another advantage of SAXS appears in late stages of the multilayer degradation, because SAXS can better recognize bits of the multilayer structure. The XRD patterns taken on annealed samples are soon dominated by diffraction lines coming from coherent parts of the multilayer, which overshadow the superstructure satellites. This makes the calculation of parameters of the multilayer model from the XRD pattern nearly impossible.

6. Conclusions

Diffraction experiments done on Fe/Au multilayers confirmed that combination of SAXS and wide-angle XRD is an efficient tool to study the real structure of highly disturbed periodic multilayers. The main advantage of that combination appeared especially in multilayers with interface discontinuities. XRD and SAXS were similarly sensitive to the early stages of the multilayer precipitation, although the reflectivity curves and XRD patterns were affected by interface discontinuity in different manners. This is because XRD recognized better the degree of crystallinity of the layers and because the re-crystallization starts without any influence on the interface continuity. At longer annealing time, the effect of the interface discontinuity on the XRD pattern became rather strong. Thus, XRD could not see remains of a multilayer structure, which were better recognized by SAXS.

The structural changes in multilayers were induced by successive annealing at 200 and 300 °C. The superstructure of the multilayer with thin iron and gold layers (26 Å/24 Å) × 10 was completely damaged after annealing for 2 h at 200 °C followed by annealing for 2 h at 300 °C. Nevertheless, SAXS could still identify the periodicity of precipitates. The multilayer with the thick iron layer, Fe/Au (70 Å/21 Å) × 13, survived the annealing for 2 h at 300 °C, which was preceded by annealing for 2 h at 200 °C. In both kinds of multilayer, the structural changes began with re-crystallization of individual layers followed by increase of the interface discontinuity and ended with precipitation of the layers.

Acknowledgments

DR appreciates the support of this work through the Alexander von Humboldt Fellowship. The authors thank Professor R Krishnan and Dr A Das (CNRS, Versailles, France) for supplying samples of Fe/Au multilayers.

References

[1] Fullerton E E, Schuller I K, Vanderstraeten H and Bruynserade Y 1992 *Phys. Rev.* B **45** 9292
[2] Underwood J H and Barbee T W 1981 *Appl. Opt.* **20** 3027
[3] Holý V and Baumbach T 1994 *Phys. Rev.* B **49** 10668
[4] Rafaja D, Chládek M, Valvoda V, Seddat M, Lassri H and Krishnan R 1997 *Thin Solid Films* **292** 61
[5] Rafaja D, Vacínová J and Valvoda V 2000 *Thin Solid Films* **374** 10
[6] Berkowitz A E, Mitchell J R, Carey M J, Young A P, Spada F E, Parker F T, Hütten A and Thomas G 1992 *Phys. Rev. Lett.* **68** 3745
[7] Xiao J Q, Jiang J S and Chien C L 1992 *Phys. Rev. Lett.* **68** 3749
[8] Öksüzoglu R M, Elmali A, Weirich T E, Fuess H and Hahn H 2000 *J. Phys.: Condens. Matter* **12** 9237
[9] Luby Š, Majková E, Špásová M, Jergel M, Senderák R, D'Anna E, Luches A, Martino M, Brunel M and Dmitrenko I M 1998 *Thin Solid Films* **312** 15
[10] Wang W, Zhu F, Lai W, Wang J Q, Yang G, Zhu J and Zhang Z 1999 *J. Phys. D: Appl. Phys.* **32** 1990
[11] Hecker M, Tietjen D, Elefant D, Schneider C M, Qiu A, Cramer N, Camley R E and Celinski Z 2001 *J. Appl. Phys.* **89** 7113
[12] Wang J Q and Xiao G 1994 *Phys. Rev.* B **49** 3982
[13] Ge S, Li H, Li C, Xi L, Li W and Chi J 2000 *J. Phys.: Condens. Matter* **12** 5905
[14] Errahmani H, Berrada A, Schmerber G and Dinia A 2002 *J. Magn. Magn. Mater.* **238** 145
[15] Zhang S and Levy P M 1993 *J. Appl. Phys.* **73** 5315
[16] Rafaja D, Fuess H, Šimek D, Kub J, Zweck J, Vacínová J and Valvoda V 2002 *J. Phys.: Condens. Matter* **14** 5303
[17] Massalski T B, Subramanian P R, Okamoto H and Kacprzak L 1990 *Binary Alloy Phase Diagrams* 2nd edn (Materials Park, OH: ASM International)
[18] Born M and Wolf E 1999 *Principles of Optics* 7th edn (Cambridge: Cambridge University Press)
[19] James R W 1965 *The Optical Principles of Diffraction of X-Rays* (New York: Cornell University Press)
[20] Parratt L G 1954 *Phys. Rev.* **95** 359
[21] Névot L and Croce P 1980 *Rev. Phys. Appl.* **15** 761
[22] Sinha S K, Sirota E B, Garoff S and Stanley H B 1988 *Phys. Rev.* B **38** 2297
[23] Holý V, Kuběna J, Ohlídal I, Lischka K and Plotz W 1993 *Phys. Rev.* B **47** 15896
[24] Rauscher M, Salditt T and Spohn H 1995 *Phys. Rev.* B **52** 16855
[25] Krishnan R, Das A and Porte M 1997 *J. Magn. Magn. Mater.* **168** 15
[26] Holý V, Pietsch U and Baumbach T 1999 *High Resolution X-Ray Scattering from Thin Layers and Multilayers (Springer Tracts in Modern Physics vol 149)* (Berlin: Springer)
[27] PDF-2 on CD-ROM 2001 (Newtown Square, PA: JCPDS-ICDD)